Conférence Internationale en Automatique & Traitement de Signal (ATS-2017)
Proceedings of Engineering and Technology – PET
Vol.23pp.22-27

Advanced Wavelet Transform for Broken Rotor Bar Detection in Induction motor

Keskes Hassen[#1], Ahmed Braham[#1*2]

[#1] Research laboratory: Matériaux, Mesures et Applications (MMA), INSAT, Tunis
[*2]Applied Sciences and Technology National Institute (INSAT), *Carthage University*
[1]keskes.hassen@gmail.com
[2]ahmed.brahm@insat.rnu.tn

***Abstract*—This paper deals with faults diagnosis of induction motors (IM) based on advanced wavelet transform technic namely recursive stationary wavelet packet transform (RSWPT). Most often, broken rotor bar (BRB) frequency components are hardly detected in the stator current due to its low magnitude and its closeness to the supply frequency component. Compared to the traditional wavelet transforms technics, RSWPT can eliminate completely the fundamental frequency. The use of a lower sampling rate is an important factor to optimize the cost and the computation time of the diagnosis systems. The experimental results show that the proposed methods have a good performance to detect BRB under different load conditions and different fault severity.**

***Keywords*— Fault detection, Induction Motor, Broken-Rotor-Bar, Wavelet Transforms.**

I. INTRODUCTION

The IM has dominated the field of electromechanical energy conversion due to its robustness and the convenient power weight ratio. Despite its robustness, the IM presents some faults such as BRB [1-5]. This failure has become an important issue in the field of fault diagnosis. Indeed, operating IM with BRB may not only damage the motor itself, but can also have a catastrophic impact on the related machines. The BRB fault introduces sideband component around the fundamental frequency in the current spectrum [1-4]. The frequency fault is given by $f_b = (1 \pm s) f_f$, where f_b is the sideband frequency associated to the BRB, s is the motor slip per unit and f_f is the fundamental frequency. The Motor Current Signature Analysis (MCSA) is one of the most used techniques in IM fault detection [1-4]. The main purpose of MCSA is to analyze the stator current and detect the current harmonics related to the fault [1-4]. The MCSA is nearly used to extract the sensitive feature related to the fault. Filippetti et al. [5] estimated the amplitude of the BRB frequency by FFT. However, the spectral leakage can make the frequency fault detection difficult under slow motor slip. Ayan et al. [6] improved this inconvenience by using Welch power spectral density (PSD) estimation as a feature extraction method with sampling frequency f_s of 10 kHz and number of samples N_s of 20 000 samples. The experimental results showed that the proposed method is able to detect the faulty conditions with high accuracy. Notwithstanding, this approach requires a steady-state operating condition. To overcome this problem Sadeghian et al. [7] presented an algorithm based on wavelet packet transform with f_s = 1920 Hz and N_s = 9984 samples. However, the method needed slip estimation which has made the automatic detection difficult. To overcome this problem Kia [8] applied Discrete Wavelet Transform (DWT) to the space-vector magnitude of the stator phase current and computed the coefficient energy associated to the rotor fault with f_s = 10 Khz and N_s = 65536 samples. This approach was successfully tested with different load level. Nevertheless, the use of the space-vector current requires three current sensors which made detection more expensive. Bouzida [9] employed one current sensor and DWT to detect BRB under with f_s = 10 Khz and N_s = 100000 samples. Yet, all these methods required good knowledge of the signals to find the correct f_s and N_s to improve the detection of faults [5-7]. As a matter of fact, the sampling rate and number of samples are closely related to the fault detection performance. In addition, the use of a low sampling rate and a small number of samples mean less computation time, which could lead to more effective and less expensive embedded system design for motor condition monitoring applications [10].

This paper aims to evaluate BRB feature extraction performance of a novel wavelet technique namely RSWPT. Compared to the traditional feature extraction techniques such as DWT and (Wavelet Packet Transform) WPT, RSWPT eliminates entirely the fundamental frequency, does not affect the fault frequency components, and provides only one sensitive descriptor for arbitrary load under a lower sampling rate of 224 Hz and 1024 samples. The energy of the descriptor is statistically evaluated using a boxplot.

The reminder of this paper is organized as follows: section 2 recalls RSWPT technique. Section 3 describes the experimental setup. Section 4 evaluates the RSWPT feature extraction performance. Section 5 concludes the findings of this paper.

II. RECURSIVE STATIONARY WAVELET PACKET TRANSFORM

The DWT is widly used in signal processing, image analysis, telecommunication and failure forecasting techniques [11]. Mallat's pyramid algorithm which is deemed to be an important algorithm for computing the DWT coefficients consists of a collection of high-pass (H) and low-pass (L) filters giving two coefficients namely details and approximations. In the next decomposition levels, the filters are only applied to the approximations. Compared with DWT,

the Wavelet packet transform (WPT) decomposes recursively the details and approximations coefficients, thus constructing a tree-structured multiband extension of the wavelet transform [11]. The main drawback of WPT and DWT is the subsampling which reduces the temporal resolution. To get around this inconvenience and keep all coefficients samples, SWPT is performed to eliminate the subsampling in each level. Fig. 1 shows two levels SWPT decomposition tree for two levels. The frequency range of the SWPT coefficients is shown in Fig. 2. It can be calculated by $\left[\frac{nf_s}{2^{j+1}}, \frac{(n+1)f_s}{2^{j+1}}\right]$.

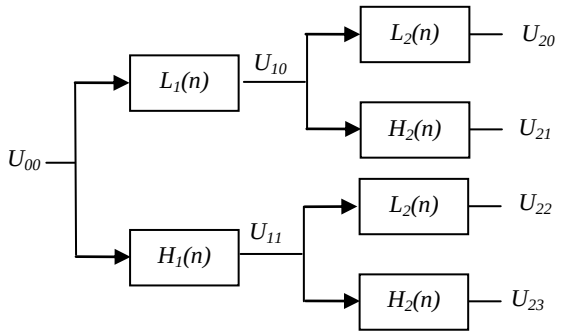

Fig. 1. The SWPT decomposition tree for two levels.

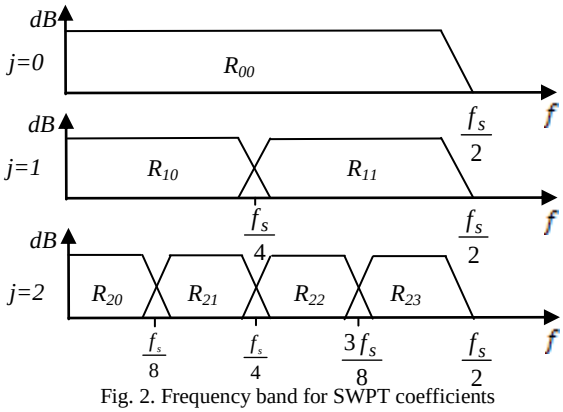

Fig. 2. Frequency band for SWPT coefficients

In many applications WPT and SWPT can't filter completely the adverse frequency around the wavelet coefficient frequency bandwidth [12]. In order to improve the quality factor of SWPT filter a new algorithm based on RSWPT is proposed, see Fig. 3. Q is defined by the following equation $\Delta f = \frac{f_0}{Q}$ Where f is the center frequency of the coefficient and Δf is the frequency bandwidth between the -3 dB points located on either side of the center frequency. (Q_{acc}) is the acceptable Q factor. k is number of SWPT decomposition.

Expression of SWPT (1) and (2) can be rewritten as

$$R_{j+1,2n}(t) = H_{j+1}(t) * R_{j,n}(t) \quad (1)$$

$$R_{j+1,2n+1}(t) = L_{j+1}(t) * R_{j,n}(t) \quad (2)$$

The Convolution Theorem gives

$$r_{j+1,2n}(f) = h_{j+1}(f) \times r_{j,n}(f) \quad (3)$$

$$r_{j+1,2n+1}(t) = l_{j+1}(f) \times r_{j,n}(f) \quad (4)$$

The RSWPT is mathematically expressed as

$$R^k_{j+1,2n}(f) = u_{j,n}(f) \times \left(h_{j+1}(f)\right)^k \quad (5)$$

$$R^k_{j+1,2n+1}(f) = u_{j,n}(f) \times \left(l_{j+1}(f)\right)^k \quad (6)$$

Fig. 4 show a theoretical example shape of the frequency response of RSWPT filters at k level 1, 2 and 3. It can be seen that $Q_{k=1} < Q_{k=2} < Q_{k=3}$ The RSWPT can highly improve the quality factor of UWPT filter.

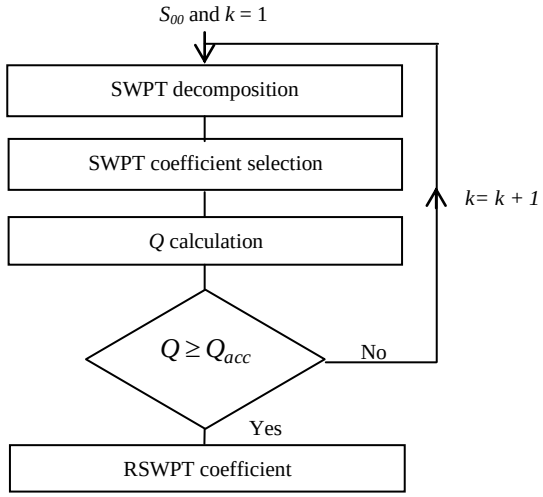

Fig. 3. RSWPT based algorithm.

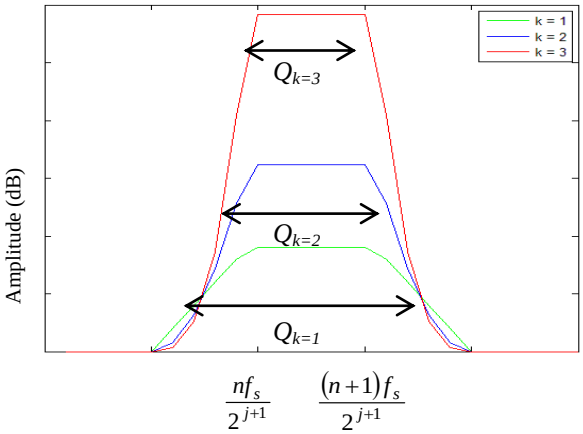

Fig. 4. RSWPT filters at k level 1, 2 and 3.

III. Experimental Setup and Feature Extraction Performance

In order validate the proposed method, experiment tests were performed with squirrel-cage IM which characteristics are 4 poles, 50 Hz, 380V, 1.7A and 0.75 HP. The experimental setup consists of IM, a load DC motor, current amplifier and sensors, see Fig. 5. The IM is tested under healthy rotor, one and two BRB under f_s = 224 Hz and N_s=1024 samples, see Fig. 6. For each individual case, 15 sets of motor-current data were collected with different load conditions namely 25%, 50%, 75% and 100%.

Fig. 5. The experimentation setup.

Fig. 6. Rotor with two broken bars.

IV. Feature Extraction Performance

In fact, the BRB introduces a frequency component given by $f_b = (1 \pm 2s) f_f$ [1]-[5]. The slip value is varied from 1.7 to 6.3%. Therefore, the left affected frequency range is [43.7, 48.3 Hz]. Using f_s = 224 Hz, the coefficients of DWT which cover the faulty frequency bandwidth are C_{a1} [0, 56 Hz], and C_{d2} [23, 56 Hz]. The existence of f_f in all DWT features makes this technique inappropriate for fault diagnosis. Fig. 7 shows a part of RSWPT and WPT tree decomposition for four levels where the gray cell corresponds to the coefficient which cover the faulty frequency bandwidth. The f_f is filtered which makes the coefficient very sensitive to the fault. Using WPT, at level 4, the length of signal will be $1024/2^4$ = 64 samples consequently the WPT cannot be used for BRB detection. RSWPT has better temporal resolution than WPT because it is implemented without subsampling.

In RSWPT the filter frequency response heavily depends on the mother wavelet. Sadeghian et al. [9] demonstrated that all mother wavelets present comparable feature extraction in BRB detection. In this work the approximation of Meyer mother Wavelet is used. Figs. 8 and 9 present PSD Welch estimate of $R^1_{4,47}$ and $R^4_{4,47}$ under 50% of load. The $R^1_{4,47}$ PSD shows that the amplitude of f_f is reduced but is not entirely filtered. In spite of the BRB sideband frequency are very close to the f_f and their magnitudes are considerably small, RSWPT at level four $R^4_{4,47}$ remove completely f_f and improve significantly the detection performance.

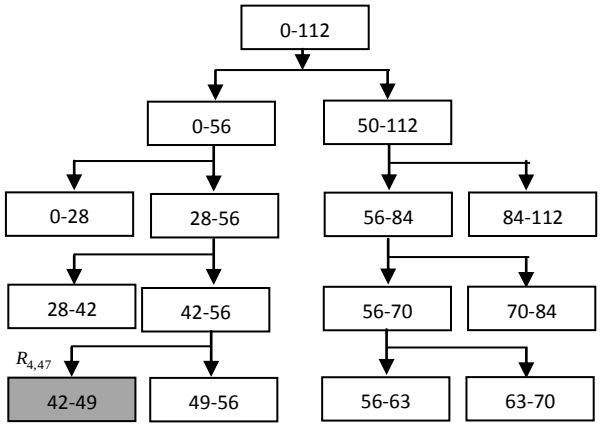

Fig. 7. RSWPT tree decomposition for four levels.

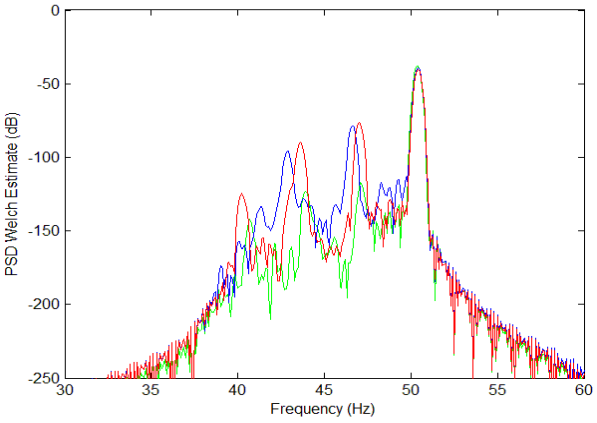

Fig. 8. PSD Welch estimates of $R^1_{4,47}$.

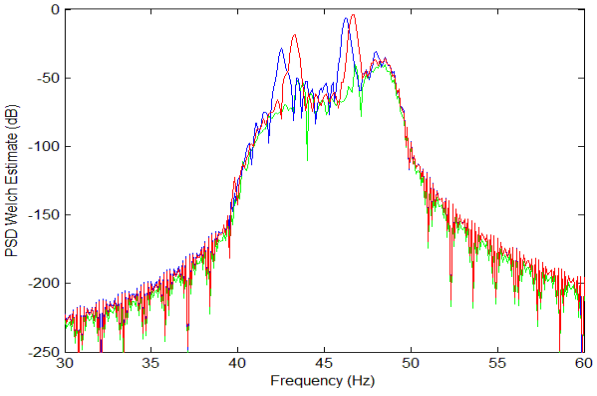

Fig. 9. PSD Welch estimates of $R^4_{4,47}$.

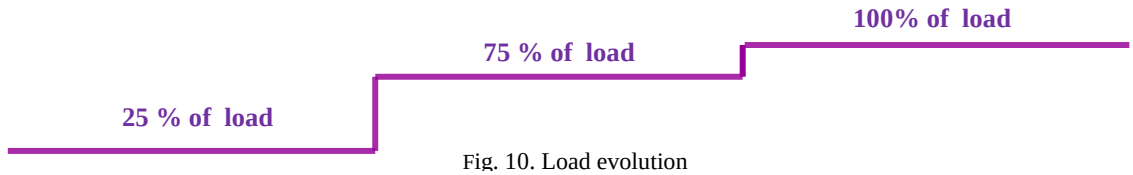

Fig. 10. Load evolution

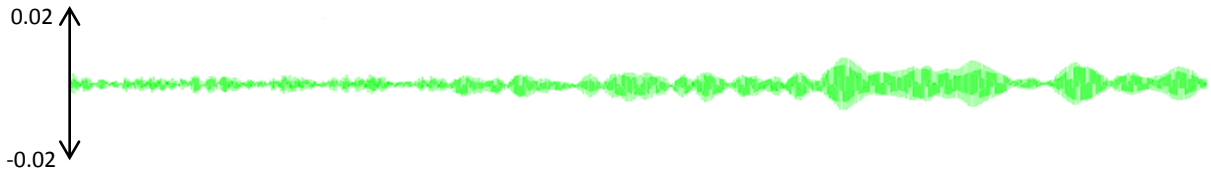

Fig. 11. $R^4_{4,47}$ evolution for HLT

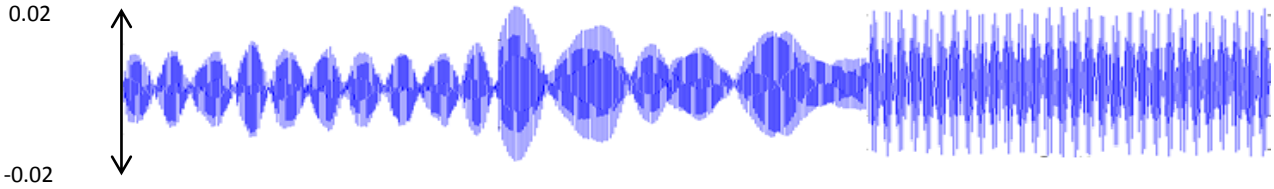

Fig. 12. $R^4_{4,47}$ evolution for 1 BRB

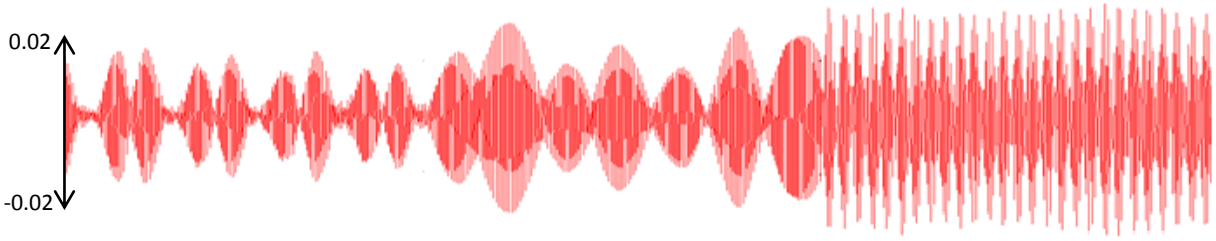

Fig. 13. $R^4_{4,47}$ evolution for 2 BRB

The $R^4_{4,47}$ evolution at a load of 25%, 75% and 100% for a HLT, one and two BRB are shown in Figs. 11, 12 and 13. For HLT conditions, $R^4_{4,47}$ is very small, while under one and two broken rotor bar, the parameter amplitude is increasing with the load. At different load levels, there is a direct relation between $R^4_{4,47}$ and the fault severity. These differences in the feature amplitude between HLT, faulty motor conditions show that they can be applied for broken rotor bar diagnosis.

In order to show the feature extraction performance of PSWT, the Matlab Statistics Toolbox is used to generate a boxplot of $R^4_{4,47}$ energy. The main advantage of the boxplot is its ability to compare two populations without knowing anything about the underlying statistical distributions of those populations. Figs. 16, 17, 18 and 19 depict the boxplot of $R^4_{4,47}$ energy under a load of 25%, 50%, 75%, and 100% respectively. It's clear that the energy median of HLT, 1BRB and 2BRB is different. It can be concluded that $R^4_{4,47}$ has a good sensibility of BRB default.

The distance between the different medians (M) gives an idea about the discrimination ability of this diagnosis parameter. $M_{25\%;HLT\_1BRB}$, $M_{50\%;HLT\_1BRB}$, $M_{75\%;HLT\_1BRB}$ and $M_{100\%;HLT\_1BRB}$ are defined as the difference between the median of HLT and 1 BRB energy under 25%, 50%, 75% and 100% load respectively. Observe that $M_{25\%;HLT\_1BRB} < M_{50\%;HLT\_1BRB} < M_{75\%;HLT\_1BRB} < M_{100\%;HLT\_1BRB}$. Thus, the heavier load condition provides better discrimination ability than the lighter load condition. On the other hand, it can be observed that the medians related to 2BRB are always greater than those of 1BRB. Therefore, there is a direct relation between the energy of the feature coefficients and the severity of the faults. However $M_{25\%;1BRB\_2BRB}$ are relatively small and the overlap between the box of 1BRB and 2BRB is not very large. Hence, it is difficult to make a difference between 1BRB and 2BRB under light loads.

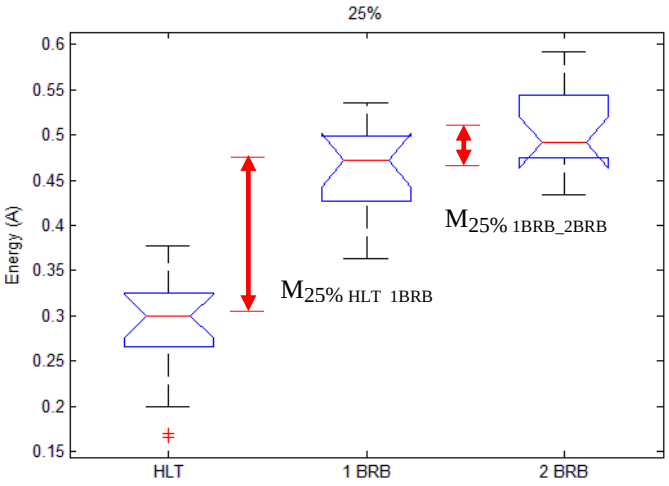

Fig. 14. Distribution of $R^4_{4,47}$ under 25% of load.

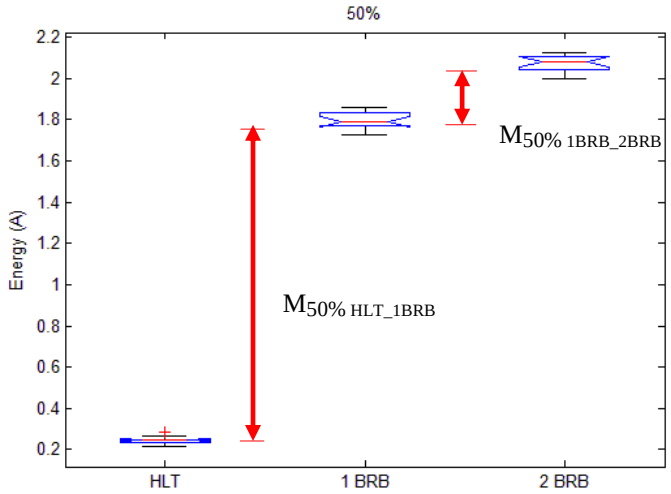

Fig. 15. Distribution of $R^4_{4,47}$ under 50% of load

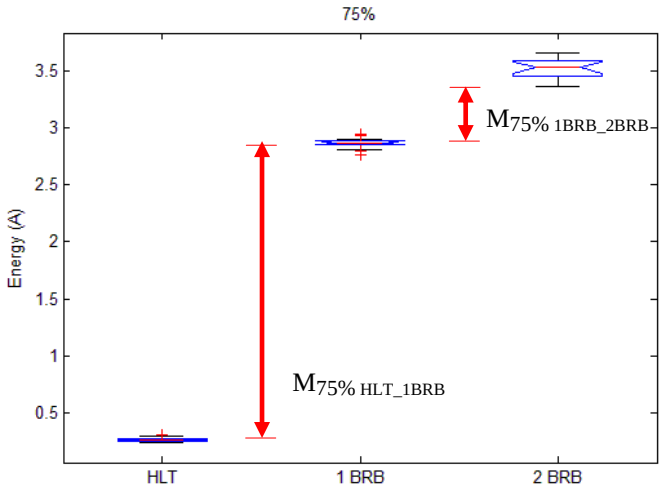

Fig. 16. Distribution of $R^4_{4,47}$ under 75% of load.

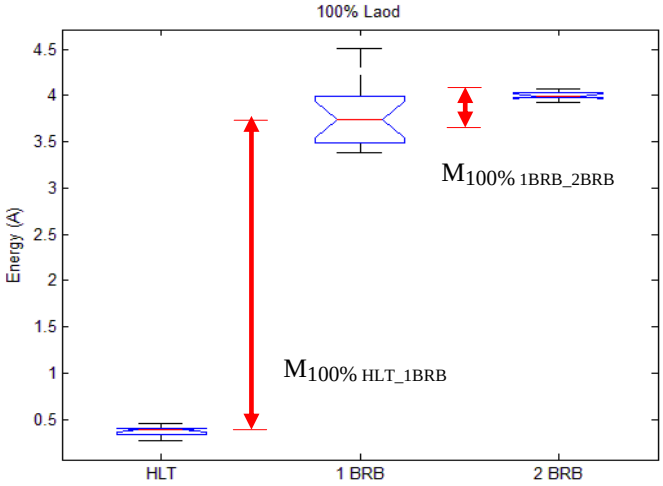

Fig. 17. Distribution of $R^4_{4,47}$ under 100% of load

V. CONCLUSION

In this paper, the RSWPT technique is applied and lower sampling rate for a fault diagnosis of broken-rotor-bar under different load conditions. The use of a lower sampling rate is an important factor to optimize the cost and the computation time of the diagnosis embedded systems. The energy of the RSWPT coefficients affected by the BRB default was proposed as the diagnosis parameter. The statistical analysis illustrate that RSWPT presents a good feature extraction performance. Based on this technique, new experiments are under development to diagnosis other faults of motor such eccentricity and bearing defects.

REFERENCES

[1] W. T. Thomson and M. Fenger, "Current signature analysis to detect induction motor faults," *IEEE Trans Ind Appl*, vol. 7, no. 4, pp. 26–34, 2001.

[2] N. Subhasis, H. Toliyat and X. Li, "Condition monitoring and fault diagnosis of electrical motors – a review," *IEEE Trans Energy Conver*, vol. 20, no 4, pp. 719–29, 2005.

[3] M.E.H. Benbouzid and G.B. Kliman, "What stator current processing-based technique to use for induction motor faults diagnosis?," *IEEE Trans Energy Conver*, vol. 18, no. 2, pp. 238–244, 2003.

[4] A. Lebaroud and A. Medoued, "Online computational tools dedicated to the detection of induction machine faults," *Electrical Power and Energy Systems*, vol. 44, pp. 752–757, 2013.

[5] F. Filippiti, G. Franceschini, C. Tassoni and P. Vas, "Recent Developments of Induction Motor Drives Fault Diagnosis Using AI Techniques," *IEEE Trans Ind Appl*, vol. 47, no. 5, pp. 994-1004, 2000.

[6] B. Ayhan, M. Chow and M. Song, "Multiple Discriminant Analysis and Neural-Network-Based Monolith and Partition Fault-Detection Schemes for Broken Rotor Bar

in Induction Motors," *IEEE Trans Ind Appl*, vol. 53, no. 4, pp. 1298-1308, 2006.

[7] A. Sadeghian, Ye. Zhongming and W. Bin, "Online Detection of Broken Rotor Bars in Induction Motors by Wavelet Packet Decomposition and Artificial Neural Networks," *IEEE Trans On Instrum and Measu*, vol. 58, no. 7, pp 2253–2263, 2009.

[8] S. H. Kia, H. Henao and G.A. Capolino, "Diagnosis of broken-bar fault in induction machines using discrete wavelet transform without slip estimation," *IEEE Trans Ind Appl*, vol. 45, no. 4, pp. 1395-1404, 2009.

[9] A. Bouzida, O. Touhami, R. Ibtiouen, A. Belouchrani, M. Fadel and A. Rezzoug, "Fault Diagnosis in Industrial Induction Machines through Discrete Wavelet Transform," *IEEE Trans Ind Electron*, vol. 58, no. 9, pp. 4385 – 4395, 2011.

[10] B. Ayhan, H.J. Trussell,M.Y. Chow and M.H. Song, "On the use of a lower sampling rate for broken rotor bar detection with DTFT and AR-based spectrum methods," *IEEE Trans Ind Electron*, vol. 55, no. 3 pp. 1421–1434, 2008.

[11] S. Mallat, *A Wavelet Tour of Signal Processing The Sparse Way*, Academic press, United States, 2009.

[12] H. Keskes, A. Braham and Z. Lachiri, "Broken rotor bar diagnosis in induction machines through stationary wavelet packet transform and multiclass wavelet SVM," *Electric Power Sys Res*,vol. 97, pp. 151–157, 2013.

ISSN 2356-5608